Earth and Planetary Science Letters 304 (2011) 520–526

Contents lists available at ScienceDirect

Earth and Planetary Science Letters

journal homepage: www.elsevier.com/locate/epsl

Direct dating of Eocene reverse faulting in northeastern Tibet using Ar-dating of fault clays and low-temperature thermochronometry

Alison R. Duvall [a,*], Marin K. Clark [a], Ben A. van der Pluijm [a], Chuanyou Li [b]

[a] Dept of Geological Sciences, University of Michigan, Ann Arbor MI, USA
[b] State Key Laboratory of Earthquake Dynamics, Institute of Geology, CEA, Beijing, China

ARTICLE INFO

Article history:
Received 28 September 2010
Received in revised form 15 February 2011
Accepted 15 February 2011

Editor: T.M. Harrison

Keywords:
Tibet
fault gouge
Ar-dating
thermochronometry

ABSTRACT

Paired together, fault gouge dating and low-temperature thermochronometry overcome the limitations and assumptions inherent in each independent technique. Here we establish timing of brittle faulting along the West Qinling fault of northeastern Tibet by dating several size fractions of fault gouge clay that represent variable populations of illite polytypes. Results show that the authigenic or fault-generated component of illite formed at 50 ± 8 Ma and that the detrital component formed at 236 ± 7 Ma indicating a Middle Eocene age of faulting and a Middle Triassic age of the wall rocks. Comparing this dataset with published thermochronology from hanging wall rocks supports the interpretation that the West Qinling fault initiated at ~50 Ma and continued until at least Middle Miocene time and that authigenic clay growth occurred at ambient temperatures of ~110 °C. Lack of overprinting of younger clay ages at this site may indicate that rocks were out of the thermal window for authigenic clay formation during later faulting episodes. The potential for temperature to control illite growth has implications for interpretation of authigenic illite ages and their relationship to deformation episodes within fault zones.

© 2011 Elsevier B.V. All rights reserved.

1. Introduction

Measurements of timing and rates of upper crustal deformation are central in the ongoing debate regarding the relative roles of tectonics and climate in mountain building (Whipple, 2009; Willett, 1999). However, a paucity of independent measures of fault motion, erosion, and elevation change in active orogens hinders progress in understanding the complex interaction of these competing processes (Whipple, 2009). Dating fault motion in particular is challenging because offsets of stratigraphic units useful in determining fault timing are not always preserved and stratigraphic ages are often poorly constrained. Thus, isotopic dating of clays in fault gouge provides an important alternative to directly date brittle fault motion because the energetics of faulting and fluid flow promotes growth of authigenic clay during faulting episodes within the shallow crust.

Fault gouge clays are assumed to comprise a two population mixture of mica polytypes: (1) detrital illite ($2M_1$) derived from wall rocks and (2) authigenic or in situ illite ($1M_d$) formed within the brittle fault zone during faulting. Isolation of pure authigenic clay for isotopic analysis is typically not possible (Grathoff et al., 2001; Pevear, 1992). As a result, ages from different clay size fractions that contain different relative percentages of each clay polytype are used to determine the age of the pure authigenic clay assuming a two-end member mixing model (Haines and van der Pluijm, 2008; Solum et al., 2005; van der Pluijm et al., 2006).

Because fault ages calculated using the two-end member mixing model correspond to discrete events that represent either the timing of short-lived faulting or a finite period of fluid-present fault motion (Haines and van der Pluijm, 2008; Solum et al., 2005; van der Pluijm et al., 2006), determining the complete history of fault activity from a single fault-gouge age is unlikely. Illite ages determined for faults with prolonged histories are thought to represent the last major period of fault motion assuming that new authigenic illite growth occurs with each successive faulting event and the complete overprinting of illite grown during the earlier phases of deformation (Solum et al., 2005; Haines and van der Pluijm, 2008). Whether such assertions should apply to all cases, however, remains largely untested.

The conditions under which authigenic clay forms in a fault zone are critical to the interpretation of illite ages. Temperature is likely to be one of the key parameters controlling its growth but due to limited temperature data within fault zones dated using the illite age analysis technique, the growth temperature of authigenic illite in fault gouge is not well constrained. Early experimental work and studies of basin brines suggest that the $2M_1$ polytype grows above 280 °C and that it is the most stable phase (Velde, 1965), whereas the $1M_d$ polytype is thought to form at significantly lower temperatures below 200 °C (Grathoff et al., 2001; Velde, 1965). If the window of growth temperatures of authigenic illite is relatively narrow, then the range of fault depths where formation can occur will also be limited. Importantly, in this case, there will be a relationship between depth

* Corresponding author.
E-mail address: duvall@umich.edu (A.R. Duvall).

0012-821X/$ – see front matter © 2011 Elsevier B.V. All rights reserved.
doi:10.1016/j.epsl.2011.02.028

and age of fault events and, specific periods of fault motion (i.e. first or last slip event or some stage in between) could be targeted for sampling if exhumation history along the fault is independently known.

In this study, we determine timing of fault motion using $^{40}Ar/^{39}Ar$ dating of illite in fault gouge for a major reverse fault in northern Tibet where the erosional history from thermal data is precisely known (Clark et al., 2010). There are several advantages to combining results from fault gouge dating with thermochronometry at the same location. Cooling histories from thermochronometry place important constraints on the temperature of authigenic illite growth and thus interpretation of gouge ages. Additionally, comparison of thermal histories with gouge ages from a single or multiple faults offers independent information on the timing of discrete fault events along specific structures that relate to range growth, and may also provide separate evidence for potential erosional periods that are related to climate rather than fault motion.

2. West Qinling field site, northeastern Tibetan Plateau

Recent work in northern Tibet has shown that thrust faulting initiates at around the time of collision, which is significantly earlier than previously thought. Observations of an early, collision-age deformation history are not predicted simply by existing end-member descriptions of plateau formation (Clark, in review; Clark et al., 2010; Dayem et al., 2009; Kong et al., 1997). Although continuum (England and Houseman, 1986) and step-wise growth (Tapponnier et al., 2001) models of Tibet are widely cited as contrasting end members for plateau development, they share the view that edge forces resulting from India's northward advance into Asia (collision circa 50 Ma, Rowley (1996)) produced high strain rates and crustal thickening that first accumulates at the plate boundary and then propagates outward in time. Mid-to-late Miocene compressive structures along the distal, northeastern plateau margin (Fig. 1) are well documented (Fang et al., 2005; Lease et al., 2007; Meyer et al., 1998; Zheng et al., 2006). Additionally, regional deformation at or near collision time is implied by clock-wise rotations up to 40° and onset of basin deposition between 55 and 52 Ma in the greater Xining basin region (Dai et al., 2006; Dupont-Nivet et al., 2004; Horton et al., 2004) and by at least 29 Ma in the Linxia basin (Fang et al., 2003), as well as by low-temperature thermochronology (Clark et al., 2010) and structural observations (Yin et al., 2008) that indicate Eocene activity along major northern Tibet thrust structures (Fig. 1).

We compare the fault gouge age results with the thermal history of hanging wall rocks along a segment of the West Qinling fault in northeastern Tibet (Fig. 1) where the slip history likely took place along only a single strand. Eocene thrust activity is proposed along this fault, which is one of the longest and most continuous structures within the northern margin of the plateau. Recently published apatite (U–Th)/He ages (closure temperature of 60–70 °C) from samples collected along a single depth transect show an interval of steep age/depth gradient starting at ~45–50 Ma and continuing through at least 12.5 Ma, which is interpreted as an increase in erosion rate of hanging wall rocks due to thrusting along the West Qinling fault (Clark et al., 2010). Assuming that faulting is the cause of accelerated erosion, Clark et al. (2010) proposed that initial rapid cooling at the West Qinling fault signals the first major thrust activity in northeastern Tibet, coincident with the timing of India–Eurasia collision. Forward thermal modeling of helium data that considers radiation damage effects on helium closure temperature and regional geologic constraints suggests sedimentary cover of up to 2 km over the West Qinling rocks during Late Cretaceous through Eocene time (Clark et al., 2010). Sediment deposition during this time implies regional lowlands and basin inversion following the initiation of the West Qinling thrust fault. We sampled gouge from a site along this fault located near the helium transect (Fig. 1). Although the fault zone is more complex to the west and east, it appears to be comparatively simple at the sample site (BGRM Gansu, 1989). Here, the moderately-dipping (~45°) reverse fault is exposed as a single strand that bounds the Linxia basin (Fig. 1). Hanging wall rocks are dominantly Middle–Late Triassic flysch deposits of the Songpan Ganzi complex and footwall rocks are primarily Neogene fine-to-coarse grained sandstones (BGRM Gansu, 1989) deposited within the Linxia basin as a result of flexural loading (Fang et al., 2003). Subsidence patterns derived from several measured stratigraphic sections (Fang et al., 2003) indicate that the basin is flexurally loaded from the south by the West Qinling fault (Fig. 1). Based on detailed magnetostratigraphy, six cycles of fining upward sedimentary sequences were deposited within the Linxia basin from at least 29 Ma through 1.7 Ma (Fang et al., 2003). Poor fossil control at the base of the deepest section prevents tighter age estimates and earlier sediment deposition may have occurred.

3. Illite age analysis

Fault dating is accomplished by measuring $^{40}Ar/^{39}Ar$ of clays in fault gouge. It is rarely possible to date 100% fault-formed clay as most size fractions of gouge material include both detrital and authigenic phases and thus comprise a mixture of grain ages (van der Pluijm et al., 2006). As a result, a mixing line of individual gouge clay size fractions that contain various percentages of authigenic clay is created to circumvent this issue. The percentage of $2M_1$ polytype plotted against apparent argon age for several size fractions is extrapolated to pure authigenic and pure detrital illite end member ages assuming that these are the only two K-bearing components within the sample (Fig. 2). Coarse (0.2–2.0 μm), medium (0.05–0.2 μm), and fine (<0.05 μm) grained clay sized fractions were prepared for analysis of gouge sampled from the fault zone (Fig. 1). All fault-rock materials were disaggregated and separated into clay-sized fractions by first gravitational and centrifugal settling, and then drying under low-heat lamps. Carbonate minerals, which obscure peaks used for polytype quantification, were removed with a weak (~1 M) acetic acid solution after separating a small aliquot of material for $^{40}Ar/^{39}Ar$ dating.

A possible complication when analyzing fine-grained crystallites is the displacement of ^{39}Ar that results from the nuclear transformation of ^{39}K. This "recoil effect" may lead to a significant loss of neutron-induced ^{39}Ar and thus produces erroneously old ages. To circumvent this issue, all clay size fractions were packaged into fused silica vials and sealed prior to irradiation, thereby retaining any ^{39}Ar expelled due to recoil (see van der Pluijm et al., 2001 for details on this glass encapsulation technique). Irradiation was performed at the McMaster University Nuclear Reactor (MNR) research facilities and Ar measurement took place at the University of Michigan. The sample vials were first broken open and the initial (recoiled) gas was analyzed followed by step-heating under a defocused laser until sample fusion occurred. Due to Ar recoil (Dong et al., 1995) and because each size fraction comprises a mixture of grain ages, the resulting age spectra from this study do not yield clear plateaus and we determine the time of faulting by plotting total gas ages rather than retention ages on the illite-age analysis plot (Fig. 2).

X-ray diffraction methods were utilized to quantify the percentage of the detrital $2M_1$ and authigenic $1M_d$ illite polytypes for each aliquot. The separate size fractions of clay were step scanned from 16 to 44 2Θ with a 0.05° step size at 30 s per step using a Scintag X-ray diffractometer at the Electron Microbeam Analysis Laboratory (EMAL), University of Michigan. We used an end-packer device similar to that described in Moore and Reynolds (1989) in order to create near-random powder mounts for scanning, which is necessary to quantify illite polytypes accurately. The relative intensity of the (002) and (020) peaks was used to determine whether randomness was achieved (Pevear, 1992). Illite polytype quantification was accomplished by using the WILDFIRE© program (Grathoff and Moore, 1996; Reynolds, 1994). Modeling of the data entailed

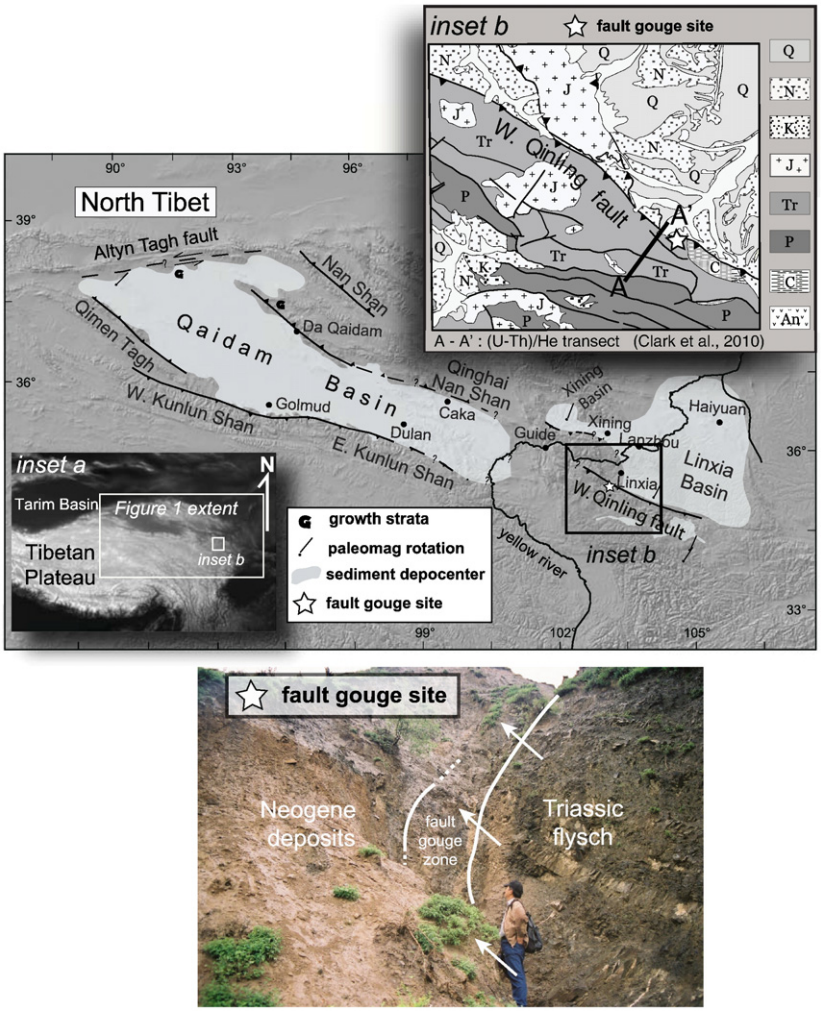

Fig. 1. Shaded relief location map of West Qinling study area in northern Tibet. Faults and basins shown are those thought to be active during the Eocene (55.8–33.9 Ma). Inset a: extent of Fig. 1 within the greater Himalaya/Tibetan Plateau region. Inset b: generalized geologic map simplified from BGMR Gansu (1989). Q—quaternary deposits, N—Neogene sandstones and shales of the Linxia basin, K—Cretaceous sandstones and shales, Tr—Triassic flysch deposits (Songpan Ganzi complex), P—Permian rocks, C—Carboniferous rocks, and An—Archean rocks. A–A′ line shows the location of the (U–Th)/He vertical transect in Clark et al. (2010). Lower frame shows a photograph of the West Qinling fault gouge sample site.

matching measured x-ray diffusion patterns for each clay size fraction with those generated using WILDFIRE© for variable populations of the two illite polytypes. Typical precision for this method is on the order of 3–5% as determined by comparing synthetic and natural samples (Haines and van der Pluijm, 2008).

4. Results

Four clay size fractions were analyzed in this study. Modeling of XRD powder patterns for each aliquot indicates 23, 45, and 63% (±3%) $2M_1$ for the fine, medium and coarse clay fractions respectively with an additional fine size fraction at 20% (±5%) (Table 1). Corresponding $^{40}Ar/^{39}Ar$ total gas ages for these aliquots are 94.1±0.5, 131.1±0.7, 170.6±0.5, and 95.2±3.2 (Table 1). A least squares regression (York, 1968) of $2M_1$ percentage versus illite Ar age constrains a 50±8 Ma (MSWD=0.6) age of the authigenic component and a 236±7 Ma (MSWD=0.9) age of the detrital component (Fig. 2). The larger errors (≤16%), calculated using a York regression (York, 1968), mostly reflect the statistics of low sample numbers compared with other similar fault gouge studies that produce repeat analyses that differ less than 2 Ma (e.g. van der Pluijm et al., 2001). Additionally, the range in percentage of illite components within the individual clay size fractions (20–65% $2M_1$ in the West Qinling sample) also affects the intercept errors.

Several assumptions are inherent in illite age-analysis. First, illite from fault-gouge samples is derived from a two end-member system (e.g. no late diagenesis) where these end-member polytypes have known and identifiable x-ray diffraction patterns. Second, we assume that authigenic illite is primarily a product of faulting at low-temperature conditions (<200 °C) and that the authigenic age represents the time of illite formation rather than a time when the sample passed through a particular thermal window or "closure temperature". In addition, we assume negligible Ar loss from the sample in nature. We consider our results in the context of these assumptions and demonstrate their reliability.

The relationship between detrital illite percentage and Ar age is useful in assessing the two end-member assumption because the percentage of detrital illite should be linearly related to age for the different clay size populations only if two distinct polytypes exist within the mixture. If authigenic and/or detrital illite components with variable argon ages due to post-faulting diagenesis, preservation of multiple phases of detrital illite from wall rocks, or multiple phases of authigenic illite grown during different faulting events are present within a single fault gouge sample, then a linear relationship between illite percentage and age is highly unlikely because more than two

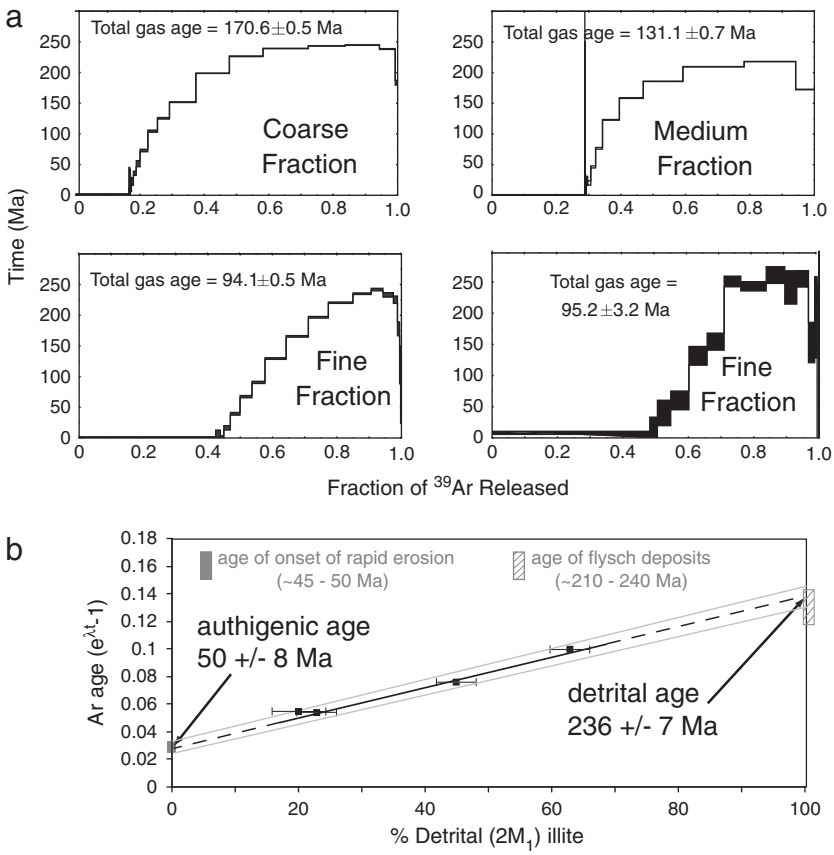

Fig. 2. a. $^{40}Ar/^{39}Ar$ results for the coarse, medium, and two fine fractions of West Qinling fault gouge. b. Illite age analysis plot for West Qinling fault rocks. Plot displays percent detrital ($2M_1$) illite versus the age (expressed as $e^{\lambda t}-1$). Black symbols represent total gas ages. Horizontal error bars represent uncertainty on $2M_1$% (precision 3–5%) (Haines and van der Pluijm, 2008), vertical error on $e^{\lambda t}-1$ is smaller than the symbol. The function $e^{\lambda t}-1$, where λ is the decay constant of argon and *t* is the apparent age, is plotted rather than age because it is the decay constant of argon that is linearly proportional to the percentage of detrital mica. 0% $2M_1$ age on the left side of the plot represents the authigenic or fault age, and the 100% $2M_1$ age on the right side of the plot is interpreted as the detrital age of wall rocks. Grey lines represent errors derived using a York regression (York, 1968). Shaded boxes represent age of onset of rapid erosion from (U–Th)/He analysis (Clark et al., 2010) and age of the Songpan Ganzi wall rocks (BGMR Gansu, 1989; Weislogel, 2008).

argon-age end members comprise the mixture. The age and $2M_1$ percentage of the size fractions from the West Qinling fault site are well fit by a linear segment and the $2M_1$ percentage correlates positively with grain size and total gas age, both of which support the two-population illite assumption (Fig. 2). Separation of finer clay size fractions would improve the error on the linear regression used to determine the authigenic age, but gouge from the West Qinling fault does not contain measurable quantities of super fine clay (≪0.05 μm). Thus, we were unable to produce a size fraction with less than 20% $2M_1$. A coarser size fraction (>65% $2M_1$) could also improve the intercept constraints, however, previous studies have shown that fractions greater in size than 2 μm are likely to be contaminated with other potassium bearing phases (e.g. potassium feldspar) and thus yield uninterpretable Ar ages (e.g. van der Pluijm et al., 2001).

Table 1
Table 1 shows the percentage of detrital ($2M_1$) illite and total gas and retentive Ar ages in Myr for the four fractions of fault gouge clays from the West Qinling fault site. Corresponding Ar release spectra are shown in Fig. 2.

Clay size (μm)	Detrital illite (%)	$^{40}Ar/^{39}Ar$ total gas age (Myr)	$^{40}Ar/^{39}Ar$ retention age (Myr)
Fine (a)	23 ± 3	94.1 ± 0.5	159.3 ± 0.8
Fine (b)	20 ± 5	95.2 ± 3.2	172.6 ± 5.6
Medium	45 ± 3	131.1 ± 0.7	181.1 ± 0.8
Coarse	63 ± 3	170.6 ± 0.5	202.4 ± 0.6

The growth of authigenic illite is assumed to be lower than the closure temperature to argon loss and thus, the authigenic illite age represents the time of formation. Here, we can estimate the temperature conditions of illite growth by comparing the authigenic illite age to the temperature history of West Qinling hanging wall rocks. One-dimensional forward thermal models of West Qinling apatite helium data constrain accelerated hanging wall erosion at 45 or 50 Ma following a period of isothermal holding since 110 Ma, assuming a layered thermal structure and using the helium closure temperature from the radiation damage model (RDAMM) kinetics of Flowers et al. (2009) (Clark et al., 2010). Fig. 3 shows the time–temperature history of West Qinling hanging wall rocks given these model results and assuming a geothermal gradient within basement rocks of 25 °C/km (grey dashed line Fig. 3) and 30 °C/km (black dashed line Fig. 3). Using this thermal history and the fault gouge age and errors, a temperature of 108 ± 10 °C is estimated at the time of authigenic clay formation (Fig. 3). Though it cannot be ruled out that fluid circulation may be responsible for a different thermal regime within the fault zone, if temperatures were similar within the fault and the hanging wall rocks, then gouge formation occurred well below the approximate 250 to 350 °C illite closure temperatures estimated using the equations of Dodson (1973) and recently published muscovite diffusion parameters appropriate for a cylindrical geometry (E = 64 kcal/mol and $D_o = 4\ cm^2/s$; Harrison et al., 2009) for effective diffusion radii of 0.05 to 2 μm and cooling rates ranging from 1 to 10 °C/Ma. This supports the notion that argon age of authigenic illite represents formation and not subsequent cooling

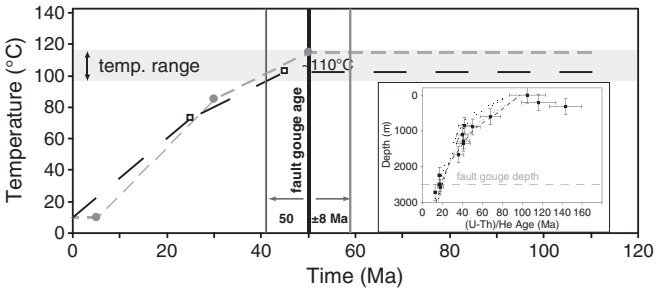

Fig. 3. Time–temperature plot of West Qinling hanging wall rocks constructed using preferred one-dimensional forward thermal models of apatite helium age data (Clark et al., 2010) for a geothermal gradient in basement rocks of 25 °C/km (grey dashed line) and 30 °C/km (black dashed line). Grey box represents temperature range of authigenic illite formation estimated by superimposing fault gouge age and errors onto these cooling profiles. Dots and squares mark cooling rate changes for each profile. Inset shows apatite helium age data for West Qinling vertical transect. Horizontal error bars represent 2σ uncertainty on mean age based on single grain replicate ages and vertical error bars represent uncertainty on elevation or depth estimate below local geomorphic surface. Preferred one-dimensional forward thermal models show accelerated hanging wall erosion at 50 Ma (grey dashed line) or 45 Ma (black dashed line) following a period of isothermal holding since 110 Ma, assuming a layered thermal structure and using the radiation damage model (RDAMM) kinetics of Flowers et al. (2009). Plot adapted from Clark et al., 2010.

and provides further information on temperature of authigenic illite growth.

5. Discussion

A fault gouge age of 50 ± 8 Ma overlaps with accelerated cooling rates of hanging wall rocks at 45–50 Ma (Clark et al., 2010) (Fig. 3). Correlation between these two datasets indicates that erosion of the hanging wall was commensurate with fault motion. Neogene-aged footwall rocks within the Linxia Basin in contact with the fault gouge (BGRM Gansu, 1989; Fang et al., 2003) (Fig. 1) suggest faulting must have occurred after the Eocene Epoch, likely during Miocene time. However, correlations of these sediments to well-dated stratigraphic sections are tenuous. Continued rapid exhumation of West Qinling hanging wall rocks until at least 12.5 Ma (the age of the deepest sample dated) supports long-lived fault activity (Clark et al., 2010). The interpolated Triassic detrital illite age also agrees well with independent geologic constraints. Footwall sandstones at the West Qinling site are likely derived from eroded Songpan Ganzi rocks in the hanging wall and thus the hanging wall and footwall have the same detrital Ar signature. Middle–Late Triassic sediments of the Songpan Ganzi complex were reportedly deposited in a thick package of ten to twenty kilometers (Weislogel, 2008), thick enough to likely reset muscovite argon ages during burial assuming an average crustal geothermal gradient. Later burial events significant enough to reset Ar are not known, however Late Triassic and Jurassic magmatism occurred regionally (Weislogel, 2008). Therefore, a Triassic detrital age at this site is expected regardless of dominant footwall or hanging wall contribution to the fault zone.

Despite evidence of a protracted West Qinling fault history, post-Eocene fault motion does not appear to be reflected in the fault gouge age. Multiple episodes of fault slip that generate more than one preserved population of authigenic illite could, in theory, be difficult to resolve using fault gouge dating of illite polytypes because different populations of $1M_d$ illite are indistinguishable by XRD analysis thus producing a pseudo end member. In such cases, the 100% authigenic illite would record a mixture of ages rather than the timing of a discrete fault event. A linear relationship between illite age and percentage of detrital component, however, requires that illite polytypes are grown in the same relative proportions during each event for all size fractions. Such conditions are extremely unlikely given the wide variability in percentage of authigenic and detrital illite for same size clay fractions in previous fault gouge studies (Haines and van der Pluijm, 2008; Haines and van der Pluijm, 2010; Solum and van der Pluijm, 2007; Solum et al., 2005; van der Pluijm et al., 2006). Thus, a well-defined linear relationship between Ar age and the percentage of illite polytype likely only results from a single fault episode. Based on West Qinling cooling history, geologic relationships at the fault gouge site, and the linear trend of the fault gouge data, we conclude that the estimated fault age records the earliest phase of fault motion, rather than an average of the fault duration or older and younger pulses that mix to form a 50 Ma age of faulting.

5.1. Implications for conditions of authigenic illite growth in fault zones

The absence of overprinting by younger fault motion suggests that conditions for illite growth existed only during a relatively short interval of fault activity (<10 Myr) at this sample site compared to the longevity of the West Qinling as an active fault bounded range (~50 Myr). High potassium (K) content, large surface area, circulating fluids, and temperatures below at least 200 °C are thought to be generally appropriate for precipitation of $1M_d$ illite (Grathoff et al., 2001; Pevear, 1992). Wall rock material at the West Qinling site is predominately made up of shales and fine-grained sandstone, which commonly have high K concentrations conducive to forming clays in fault gouge. The geologic record suggests no changes in wall rock material occurred as faulting progressed, so we expect that K was also available during later faulting events. We also assume that ample surface area for clay growth during later fault episodes existed because the fault zone would have been developed after faulting initiated during the Eocene. Fluids likely play an important role in clay gouge formation; however, determining the presence and temperature of fluids circulating during the time of fault motion is outside the scope of this study.

Wall rock temperatures derived from thermochronometry (Clark et al., 2010) suggest that the purely authigenic illite component formed at ~110 °C assuming that the fault and wall rock experienced similar thermal histories (Fig. 3). One possible explanation for the lack of overprinting of younger fault ages at this site is that rocks moved outside the thermal window suitable for illite formation as thrust faulting and erosion of uplifted hanging wall rocks progressed. In this interpretation, we expect that the later fault events are recorded in gouges not yet exhumed to the surface. Unfortunately, suitable exposures of fault gouge are rare and other sites along the fault, including along more deeply exhumed segments, have not been identified. A fault gouge study from the Sierra Mazatàn extensional core complex in Mexico (Haines and van der Pluijm, 2008) with reliable, independent temperature constraints provides an important comparison to our results. At this site, onset of faulting is deduced from the timing of rapid cooling recorded by $^{40}Ar/^{39}Ar$ of K-feldspar from ductile footwall rocks (Wong and Gans, 2003). The detrital illite age ($2M_1$) matches with the approximate timing of mylonite formation whereas the authigenic age ($1M_d$) is assumed to date the later stages of faulting because it is only slightly older than an ignimbrite that caps the mylonitic carapace (Haines and van der Pluijm, 2008). Extrapolating the K-feldspar cooling data through the brittle history of faulting, the authigenic age and errors can be used to constrain the temperature of $1M_d$ illite formation at this site to between 110° and 160 °C (Haines and van der Pluijm, 2008), which overlaps with the temperature constraint from the West Qinling fault presented here.

The authigenic illite formation temperatures estimated are similar to the thermal range of two of the most commonly applied thermochronometers, apatite helium (~60–70 °C) and apatite fission track (~110 °C). Thus, comparison among results from these techniques provides powerful means to assess upper crustal deformation. Constraints on the relatively narrow temperatures of authigenic illite

growth also permit targeted sampling of clays in fault gouge that correspond to particular periods of fault motion if the exhumation history of potential sample sites is reasonably well known.

5.2. Implications for tectonic history of the Tibetan Plateau

The depth of exhumation at the West Qinling fault site (Clark et al., 2010) predicts that the fault age measured here should correspond with the beginning of rapid cooling of hanging wall rocks. Indeed, our results show overlap between the 100% authigenic illite age and the beginning of accelerated exhumation, which indicates that faulting was a first-order control on erosion in this part of the orogen. Commonly, the erosional response to dip-slip fault motion inferred from low-temperature thermochronometry is employed as a proxy for fault motion (Wagner and Reimer, 1972). Increased fluvial incision occurs in response to faulting because accelerated rock-uplift rates in the hanging wall drive increased erosion by steepening river gradients, channel narrowing, or some combination of both (for the same discharge) (Duvall et al., 2004; Whipple, 2004; Whipple and Tucker, 1999). However, increased rates of erosion can occur solely with increased precipitation (Reiners et al., 2003) where relief is pre-existing, thereby complicating unique correlation of erosion events with faulting episodes. The combination of fault related gouge ages and thermochronometry offers an avenue by which we can circumvent the ambiguity of precipitation versus fault driven exhumation patterns.

Together, the geologic history of the West Qinling fault from clay gouge dating and thermochronometry shows an internally and regionally consistent fault history that begins in the Eocene and extends through much of the Miocene. Our result offers definitive evidence of Eocene-age reverse faulting within the northeastern Tibetan Plateau and, along with reported ages on thrust faults near the Qaidam Basin (Clark et al., 2010; Yin et al., 2008), suggests that compressive deformation across a significant portion of the northern margin of the plateau initiates within 10 Myr of the initial collision between India and Eurasia. Recent model results show that far-field lithospheric deformation due to the Indian indenter shortly after collision is permissible provided that Asian lithosphere can be approximated as a thin viscous sheet, given a strong lithosphere north of Tibet and relatively thick crust in southern Tibet at the onset of plateau building (Dayem et al., 2009). Alternatively, faulting in northern Tibet signifies the constant stress and strength conditions that characterize the orogen since collision (Clark, in review).

6. Conclusions

Dating of illite from the West Qinling fault in northern Tibet suggests thrust fault motion at ~50 Ma. This age fits well with erosional and geologic constraints from hanging wall rocks and the adjacent foreland basin. Results from this site demonstrate that the $^{40}Ar/^{39}Ar$ age of authigenic illite represents a single interval in West Qinling fault history rather than an amalgamation. Our results also show that the fault-formed illite age does not always represent the latest phase in fault motion (Haines and van der Pluijm, 2008; Solum et al., 2005) as in this case, we document the initiation of faulting. Instead, authigenic illite growth appears to be restricted to a thermal window of the fault history (108 ± 10 °C), thus the stage of faulting recorded will vary among sample sites depending, at least in part, on thermal history.

Acknowledgements

We thank Chris Hall for argon analysis in the University of Michigan's Radiogenic Isotope Geochemistry Laboratory; Sam Haines and Jim Hnat for assistance with the sample preparation and data interpretation; Anja Schleicher for guidance with XRD analysis carried out at the University of Michigan Electron Microbeam Analysis Laboratory; and Karen Vasko for assistance in the field. We also acknowledge two anonymous reviewers whose comments improved this manuscript. Support for this research was provided by the National Science Foundation, Continental Dynamics Program (EAR-0507431), the National Science Foundation of China (40234040) and by the State Key Laboratory of Earthquake Dynamics (LED2008A01).

References

Bureau Geological and Mineral Resources (BGMR) Gansu Province, 1989. Regional Geology of Gansu Province, Geological publishing house, Beijing (in Chinese, 690 pp).
Clark, M.K., *in review*. Does the crust matter? A new view of post-collisional convergence rates. Nature.
Clark, M.K., Farley, K.A., Zheng, D., Zhicai, W., Duvall, A.R., 2010. Early Cenozoic faulting of the northern Tibetan Plateau margin from (U–Th)/He ages. Earth Planet. Sci. Lett. 296, 78–88.
Dai, S., Fang, X., Dupont-Nivet, G., Song, S., Gao, J., Krijgsman, W., Langereis, C., Zhang, W., 2006. Magnetostratigraphy of Cenozoic sediments from the Xining Basin: tectonic implications for the northeastern Tibetan Plateau. J. Geophys. Res. 111. doi:10.1029/2005JB004187.
Dayem, K.E., Molnar, P., Clark, M.K., Houseman, G.A., 2009. Far-field lithospheric deformation in Tibet during continental collision. Tectonics 28. doi:10.1029/2008TC002344.
Dodson, M.H., 1973. Closure temperature in cooling geochronological and petrological systems. Contrib. Mineral. Petrol. 40, 259–274.
Dong, H., Hall, C., Peacor, D., Halliday, A., 1995. Mechanism of argon retention in clays revealed by laser 40Ar39Ar dating. Science 267, 355-259.
Dupont-Nivet, G., Horton, B.K., Butler, R.F., Wang, J., Zhou, J., Waanders, G.L., 2004. Paleogene clockwise tectonic rotation of the Xining-Lanzhou region, northeastern Tibetan Plateau. J. Geophys. Res. 109. doi:10.1029/2003JB002620.
Duvall, A.R., Kirby, E., Burbank, D.W., 2004. Tectonic and lithologic controls on bedrock channel profiles and processes in coastal California. J. Geophys. Res. 109. doi:10.1029/2003JF000086.
England, P., Houseman, G., 1986. Finite strain calculations of continental deformation II: comparison with the India–Asia collision zone. J. Geophys. Res. 91, 3664–3676.
Fang, X., Garzione, C., Van der Voo, R., Rea, D.K., Li, J., Fan, M., 2003. Flexural subsidence by 29 Ma on the NE edge of Tibet from the magnetostratigraphy of Linxia Basin, China. Earth Planet. Sci. Lett. 210, 545–560.
Fang, X.M., Yan, M.D., Van der Voo, R., Rea, D.K., Song, C.H., Pares, J.M., Gao, J.P., Nie, J.S., Dai, S., 2005. Late Cenozoic deformation and uplift of the NE Tibetan Plateau: Evidence from high-resolution magnetostratigraphy of the Guide Basin, Qinghai Province, China. Geol. Soc. of Amer. Bulletin 117. doi:10.1130/B25727.1.
Flowers, R.M., Ketcham, R.A., Shuster, D.L., Farley, K.A., 2009. Apatite (U–Th)/He thermochronometry using a radiation damage accumulation and annealing model. Geochemica Cosmochim. Acta 73, 2347–2365.
Grathoff, G., Moore, D., 1996. Clays and clay minerals, 44. 835 pp.
Grathoff, G., Moore, D., Hay, R., Wemmer, K., 2001. Origin of illite in the lower Paleozoic of the Illinois Basin: evidence for brine migration. Geol. Soc. Am. Bull. 113, 1092–1104.
Haines, S.H., van der Pluijm, B.A., 2008. Clay quantification and Ar–Ar dating of synthetic and natural gouge: application to the Miocene Sierra Mazatán detachment fault, Sonora, Mexico. J. Struct. Geol. 30, 525–538.
Haines, S.H., van der Pluijm, B.A., 2010. Dating the detachment fault system of the Ruby Mountains, Nevada: significance for the kinematics of low-angle normal faults. Tectonics 29, TC4028. doi:10.1029/2009TC002552.
Harrison, T.M., Célérier, J., Aikman, A.B., Hermann, J., Heizler, M.T., 2009. Diffusion of ^{40}Ar in muscovite. Geochim. Cosmochim. Acta 73 (4), 1039–1051.
Horton, B.K., Dupont-Nivet, G., Zhou, J., Waanders, G.L., Butler, R.F., Wang, J., 2004. Mesozoic–Cenozoic evolution of the Xining-Minhe and Dangchang basins, northeastern Tibetan Plateau: magnetostratigraphic and biostratigraphic results. J. Geophys. Res. 109. doi:10.1029/2003JB002913.
Kong, X., Yin, A., Harrison, T.M., 1997. Evaluating the role of pre-existing weakness and topographic distributions in the Indo-Asian collision by use of a thin-shell numerical model. Geology 25, 527–530.
Lease, R.O., Burbank, D.W., Gehrels, G.E., 2007. Signatures of mountain building: detrital zircon U/Pb ages from northeastern Tibet. Geology 35 (3), 239–242.
Meyer, B., Tapponnier, P., Bourjot, L., Metivier, F., Gaudemer, Y., Peltzer, G., Shunmin, G., Zhitai, C., 1998. Crustal thickening in Gansu-Qinghai, lithospheric mantle subduction, and oblique, strike-slip controlled growth of the Tibet plateau. Geophys. J. Int. 135, 1–47.
Moore, D.M., Reynolds Jr., R.C., 1989. X-ray Diffraction and the Identification and Analysis of Clay Minerals. Oxford University Press, New York. 400 pp.
Pevear, D.R., 1992. Proceedings of the 7th International Symposium on Water–Rock Interaction. 1251 pp.
Reiners, P.W., Ehlers, T.A., Mitchell, S.G., Montgomery, D.R., 2003. Coupled spatial variation in precipitation and long term erosion rates across the Washington Cascades. Nature 426, 645–647.
Reynolds Jr., R., 1994. WILDFIRE, a Computer Program for the Calculation of Three-dimensional Powder X-ray Diffraction Patterns for Mica Polytypes and their Disordered Variations. Hanover, NH.
Rowley, D., 1996. Age of initiation of collision between India and Asia: a review of stratigraphic data. Earth Planet. Sci. Lett. 145, 1–13.
Solum, J., van der Pluijm, B., 2007. Reconstructing the Snake River/Hoback Canyon segment of the Wyoming thrust belt through direct dating of fault rocks, in Whence

the Mountains? Inquiries into the evolution of orogenic systems: a volume in honor of Ray Price. Geol. Soc. Amer. Mem. 433, 183–196.
Solum, J.G., van der Pluijm, B.A., Peacor, D.R., 2005. Neocrystallization, fabrics and age of clay minerals from an exposure of the Moab Fault, Utah. J. Struct. Geol. 27, 1563–1576.
Tapponnier, P., Zhiqin, X., Roger, F., Meyer, B., Arnaud, N., Wittlinger, G., Jingsui, Y., 2001. Oblique stepwise rise and growth of the Tibet Plateau. Science 291, 1671–1677.
van der Pluijm, B.A., Hall, C.M., Vrolijk, P., Pevear, D.R., Covey, M., 2001. The dating of shallow faults in the Earth's crust. Nature 412, 172–174.
van der Pluijm, B., Vrolijk, P., Pevear, D., Hall, C., Solum, J., 2006. Fault dating in the Canadian Rocky Mountains: evidence for late Cretaceous and early Eocene orogenic pulses. Geology 34, 837–840.
Velde, B., 1965. Experimental determination of muscovite polymorph stabilities. Am. Mineral. 50, 436–499.
Wagner, G.A., Reimer, G.M., 1972. Fission track tectonics: the tectonic interpretation of fission track apatite ages. Earth Planet. Sci. Lett. 14, 263–268.
Weislogel, A.L., 2008. Tectonostratigraphic and geochronologic constraints on evolution of the northeast Paleotethys from the Songpan-Ganzi complex, central China. Tectonophysics 451, 331–345.
Whipple, K.X., 2004. Bedrock rivers and the geomorphology of active orogens. Annu. Rev. Earth Planet. Sci. 32, 151–185.
Whipple, K.X., 2009. The influence of climate on tectonic evolution of mountain belts. Nat. Geosci. 2, 97–104.
Whipple, K.X., Tucker, G.E., 1999. Dynamics of the stream-power river incision model: Implications for the height limits of mountain ranges, landscape response timescales, and research needs. J. Geophys. Res. 104. doi:10.1029/1999JB900120.
Willett, S.D., 1999. Orogeny and orography: the effects of erosion on the structure of mountain belts. J. Geophys. Res. 104. doi:10.1029/1999JB900248.
Wong, M.S., Gans, P.B., 2003. Tectonic implications of early Miocene extensional unroofing of the Sierra Mazatàn metamorphic core complex, Sonora, Mexico. Geology 31 (11), 953–956.
Yin, A., Dang, Y., Wang, L., Jiang, W., Chen, X., Gehrels, G.E., McRivette, M.W., 2008. Cenozoic tectonic evolution of the Qaidam basin and its surrounding regions (Part 1): the southern Qilian Shan-Nan Shan thrust belt and northern Qaidam basin. Geol. Soc. Am. Bull. 120, 813–846.
York, D., 1968. Least squares fitting of a straight line with correlated errors. Earth Planet. Sci. Lett. 5, 320–324.
Zheng, D.W., Zhang, P.Z., Wan, J.L., 2006. Rapid exhumation at similar to 8 Ma on the Liupan Shan thrust fault from apatite fission-track thermochronology: Implications for the growth of northeastern Tibet margin. Earth Planet. Sci. Lett. 248, 198–205.